THE ASTROPHYSICAL JOURNAL, 344:265–276, 1989 September 1

STRONG, SPATIALLY EXTENDED CO 7 → 6 EMISSION FROM LUMINOUS CLOUD CORES: W51 AND DR 21

D. T. JAFFE,[1] R. GENZEL,[2] A. I. HARRIS,[2] J. B. LUGTEN,[3,4] G. J. STACEY,[3] AND J. STUTZKI[2]

Received 1988 September 19; accepted 1989 February 7

ABSTRACT

We have mapped the 372 μm CO $J = 7 \rightarrow 6$ transition toward the luminous star-formation regions W51 and DR 21. We have also observed CO $J = 2 \rightarrow 1$ and $^{12}C^{18}O$ $J = 2 \rightarrow 1$ toward selected positions. By analyzing the CO $7 \rightarrow 6$ maps in the context of existing information on these well-studied regions, we conclude that three distinct molecular cloud components contribute to the CO $7 \rightarrow 6$ emission:

1. Warm ($T \geq 100$–250 K), dynamically active ($\Delta V \geq 20$ km s^{-1} at a level of $5KT_{MB}$) material accounts for more than 75% of the velocity integrated CO $7 \rightarrow 6$ emission from the two sources. There is at least 170 $M_\odot$ of this material in each source. It centers on or near the luminous far-IR sources DR 21 and W51 IRS 2 and extends over more than 2 pc in both cases.

2. There is warm (100–500 K), quiescent ($\Delta V = 5$–10 km s^{-1}) material associated with the H II regions in each source. This narrow line component covers less than 0.5–2 pc. It represents a small fraction of the cloud mass but dominates the cooling of quiescent molecular material. The results on the quiescent component reinforce the suggestion of Harris *et al.* that 912–1100 Å photons which penetrate the cloud are responsible for heating this gas in most luminous cloud cores.

3. Cool (20–40 K) quiescent gas overlies some of the hot material. This gas is most likely part of the more extended molecular envelope around the luminous cloud core. In DR 21, this material causes a strong central reversal in the CO $7 \rightarrow 6$ line and allows us to determine the physical conditions in the absorbing cloud.

Subject headings: infrared: sources — interstellar: molecules — nebulae: individual (W51, DR 21)

I. INTRODUCTION

The submillimeter and far-infrared rotational transitions of CO are valuable probes of the molecular interstellar medium. These high-J lines give access to molecular gas not easily observable in the millimeter CO transitions and provide new information about the gas commonly observed in the low-J lines. When combined with observations of millimeter and far-IR CO transitions, submillimeter spectral lines can give quantitative measures of temperature and density in the line emission regions. Of these lines, CO $J = 7 \rightarrow 6$ at 372 μm is the highest frequency transition accessible for ground-based observations. Since the CO $J = 7$ state lies 155 K above the ground state, maps of CO $7 \rightarrow 6$ emission trace the distribution and kinematics of warm, dense molecular gas without serious confusion by the cooler, more tenuous gas that dominates the millimeter lines. Since the population of the $J = 6$ level is very sensitive to temperature and density in cool ($T < 40$ K) gas, the degree of any self-absorption in the $7 \rightarrow 6$ line places powerful constraints on the physical conditions in cool gas.

Earlier observations of CO $7 \rightarrow 6$ and $16 \rightarrow 15$ in several sources (Jaffe, Harris, and Genzel 1987, hereafter JHG) have shown that the outflows in luminous star-formation regions contain large amounts (~ 100 $M_\odot$ in W51 IRS 2) of molecular gas at temperatures greater than or equal to 500 K. In addition to the outflows, the luminous cloud cores contain quiescent ($\Delta V = 5$–8 km s^{-1}) material at temperatures substantially (at least 2–3 times) higher than the far-IR dust temperatures, or than the temperatures inferred from low-J CO line brightnesses. The submillimeter line observations showed that cool (<20–30 K), tenuous ($<10^3$ cm^{-3}) envelopes of the cloud cores seriously affect the shapes of the low-J CO lines, but do not absorb much of the CO $7 \rightarrow 6$ from the hot region. Harris *et al.* (1987*b*) used CO $7 \rightarrow 6$ and $14 \rightarrow 13$ observations toward M17 and S106 to place the existence and the nature of the warm quiescent gas in cloud cores on a firmer, more quantitative basis. In M17, this component has a narrow line width (~ 5 km s^{-1}) and a temperature between 150 and 500 K at intermediate density ($\sim 3 \times 10^4$ cm^{-3}). It accounts for 5%–20% of the total mass in the cloud core. CO $7 \rightarrow 6$ strip maps of the M17 SW core and comparisons with low-J CO and with C^+ 158 μm emission show that the hot molecular gas is near the H II/molecular cloud interface. The spatial correlation between C II, warm CO, and C I suggests that the CO $7 \rightarrow 6$ emission traces the number of clump surfaces exposed to UV from the ionizing sources (Stutzki *et al.* 1988). The Stutzki *et al.* results require the existence of at least three quiescent components; warm gas on the surface of clumps in the cloud core, cooler (40–80 K) gas in the centers of the clumps, and cool gas in the envelope.

The success of the M17 SW study leads us to undertake similar observations in other luminous star-formation regions. We present here more extensive maps of W51 ($L = 2 \times 10^6$ $L_\odot$; Harvey *et al.* 1986) and DR 21 ($L = 1.5 \times 10^5$ $L_\odot$; Harvey, Campbell, and Hoffmann 1977), plus single-beam observations of W75 N and W75 S. The goal of the mapping program is to use morphological information together with spectroscopic information to obtain a better understanding of the nature of the different cloud components and of the overall structure of the clouds.

[1] Department of Astronomy, University of Texas at Austin.
[2] Max-Planck-Institut für Physik und Astrophysik, Institut für Extraterrestrische Physik.
[3] Department of Physics, University of California, Berkeley.
[4] Institute for Astronomy, University of Hawaii.

II. OBSERVATIONS

We observed the 806.6517 GHz (371.6474 μm) CO $7 \rightarrow 6$ transition in 1986 June and 1987 June with the 3.8 m United Kingdom Infrared Telescope on Mauna Kea and the U. C. Berkeley/Max Planck Institute for Extraterrestrial Physics Cassegrain heterodyne spectrometer (Harris *et al.* 1987*a*). The receiver consisted of a Schottky diode mixer mounted in a corner cube and cooled to 77 K, an optically pumped far-IR laser local oscillator, and quasi-optical signal coupling. The single sideband receiver temperature measured on the telescope was 9000–11,000 K. The back end was a 1024 channel acousto-optical spectrometer which covered an instantaneous bandwidth of 600 MHz (220 km s^{-1}). The telescope secondary switched at 2 Hz between the source position and a position 210 arcseconds (in 1986) or 180 arcseconds (in 1987) away. For all sources except W51 (where the secondary switched alternately to reference positions north and south of the source), the off-source positions were east and west of the map positions. The telescope pointing accuracy was better than ± 3 arcseconds and the boresight position was known to better than ± 4 arcseconds.

We determined the submillimeter atmospheric transmission by measuring the temperature of the sky at several zenith angles, assuming that the transmission has a sec (z) dependence, and that the physical sky temperature equaled the ground temperature. The transmission calculation allows for the difference in atmospheric transmission in the signal and image sidebands and for the presence of ambient temperature blockage in the beam (Harris 1986). The zenith transmission ranged from 14% to 20% in 1986 and was 40% on the one night in 1987. We determined the telescope main beam efficiency (0.31) from observations of Jupiter assuming a Planck brightness temperature of 123 K, based on the observed broadband brightness temperature (Hildebrand *et al.* 1985), corrected for PH_3 and HCN self-absorption in the signal and image sidebands (Lellouch, Encrenaz, and Combes 1984). The beamsize was 25 arcseconds full width to half-maximum. All CO $7 \rightarrow 6$ line temperatures quoted here are Rayleigh-Jeans main beam brightness temperature (T_{MB}, Harris 1988). This is the Rayleigh-Jeans temperature which would result from radiation from a uniform source which fills the main beam to the first null, corrected for atmospheric transmission, ohmic losses, and main beam efficiency. The absolute temperature scale (based on estimates of all systematic and random errors associated with the calibration) is correct to $\pm 30\%$.

We observed the 230.5380 GHz $^{12}C^{16}O$ and 219.5603 GHz $^{12}C^{18}O$ $2 \rightarrow 1$ transitions in 1987 March with the NRAO 12 m telescope on Kitt Peak.[5] We calibrated the data to the T_R^* scale (Kutner and Ulich 1981) with comparisons of the radiation temperature of the sky to an ambient temperature chopper wheel [$T_R^*(^{12}CO\ 2 \rightarrow 1] = 80$ K for Orion/KL on this scale). We checked the transmission by making sky temperature measurements at a series of zenith angles. The beamsize was 32″ FWHM. Overall pointing uncertainties were about $\pm 15''$. In order to convert from the T_R^* scale used for the CO $2 \rightarrow 1$ spectra to main beam brightness temperature, the $2 \rightarrow 1$ T_R^*'s must be multiplied by the ratio of the beam efficiency measured on the moon to the main beam efficiency (~ 2.0).

[5] The National Radio Astronomy Observatory is operated by Associated Universities, Inc., under contract with the National Science Foundation.

III. RESULTS

The main results from the W51 and DR 21 mapping observations can be summarized as follows.

1. The CO $7 \rightarrow 6$ line flux maps contain evidence for extended emission from warm, dynamically active gas (with a velocity range of 20–50 km s^{-1}) in the cores of massive molecular clouds.

2. The distribution of peak CO $7 \rightarrow 6$ main beam brightness temperature (T_{MB}) differs significantly from the distribution of optically thick emission in millimeter CO lines. The distribution of CO $7 \rightarrow 6$ T_{MB} peaks toward or at the edges of H II regions as traced by radio continuum or 20 μm dust emission. The $7 \rightarrow 6$ source sizes are smaller than the millimeter CO source sizes.

3. The new observations of individual sources as well as the mapping results confirm our earlier observation that the Planck brightness temperature of the $7 \rightarrow 6$ line is typically 1.5–3 times higher than the temperature of the millimeter CO lines toward luminous sources.

4. The line shapes and strengths vary strongly both with rotational quantum number J and with location in the source.

5. While self-absorption is generally less prominent in the CO $7 \rightarrow 6$ line than in the millimeter CO lines, in at least one case (DR 21), there is a dramatically stronger central reversal in the $7 \rightarrow 6$ line.

a) The Maps and Spectra

Figures 1 and 2 show all the CO $7 \rightarrow 6$ spectra toward W51 and DR 21, respectively. The center panel in each figure is a schematic showing the locations of various other sources of emission. Figures 3 and 4 show CO $7 \rightarrow 6$ integrated intensity and peak main beam brightness temperature maps for both sources and compare them to various other types of emission. Figures 5 and 6 compare CO $7 \rightarrow 6$ profiles near the emission peaks of W51 and DR 21 to profiles of the $^{12}C^{16}O$ and $^{12}C^{18}O$ $J = 2 \rightarrow 1$ transitions. Figures 7 and 8 show a similar profile comparison for W75 N and W75 S.

b) W51 Mapping Results

There is detectable CO $7 \rightarrow 6$ emission in W51 over the entire ~ 3 pc diameter mapped region (see Fig. 1). At the edges of the map, the integrated intensity is about half the peak value. There are significant changes in the line shapes from point to point—many spectra appear to have either a broad ($\Delta v = 15$–20 km s^{-1} FWHM) component alone or a broad component with a narrower emission spike superposed.

The map of main beam brightness temperature (T_{MB}, Fig. 3*a*) has an extended peak which connects the two beam-averaged maxima in the 20 μm and radio continuum emission within the region studied in the $7 \rightarrow 6$ line. The CO $7 \rightarrow 6$ emission extends to the southeast at the $\sim 50\%$ level to cover the region around the H_2O maser centers and compact H II region in W51 MAIN, but has no local maximum there. The 180″–210″ chopper throw used for the CO $7 \rightarrow 6$ observations did not seriously affect the measurements. Spectra taken with the two chop sizes and comparisons of spectra with reference beams east and west of the source show no measurable ($< 10\%$ of peak temperature) effect on the peak temperature distribution. The dropoff in T_{MB} ($7 \rightarrow 6$) is more rapid than the corresponding drop in our T_{MB} ($2 \rightarrow 1$) observations (Fig. 9). The $2 \rightarrow 1$ observations show a 40″ diameter region at 90% of the peak temperature and a T_{MB} ($2 \rightarrow 1$) greater than 70%–80% of the

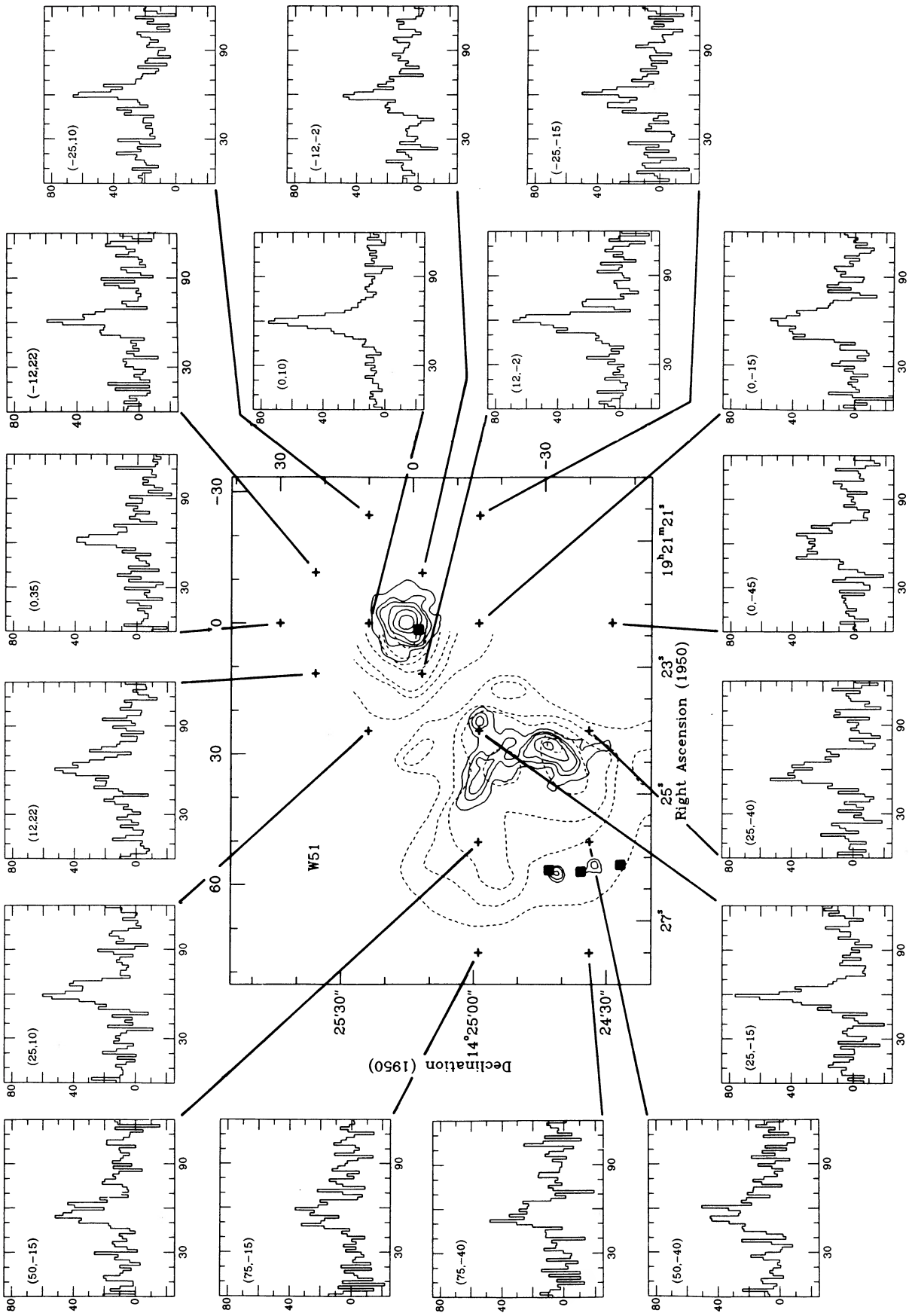

FIG. 1.—CO 7 → 6 spectra toward W51. The horizontal axis in each spectrum is velocity (km s^{-1}) relative to the local standard of rest. The vertical axis is main beam Rayleigh-Jeans brightness temperature (T_{MB}, see text). The numbers in the upper left corner of each spectrum give its position offset in arcseconds from $19^h21^m23^s.3 + 14°25'15''$ (1950). The center panel is a map of the W51 region showing the 20 μm continuum (*dashed lines:* Genzel *et al.* 1982) and the 1.3 cm continuum observed with the VLA (*solid lines:* Jaffe *et al.* 1989). The small crosses mark the positions for the CO 7 → 6 spectra and the squares mark the positions of H_2O maser emission centers (Forster *et al.* 1978; Genzel *et al.* 1982).

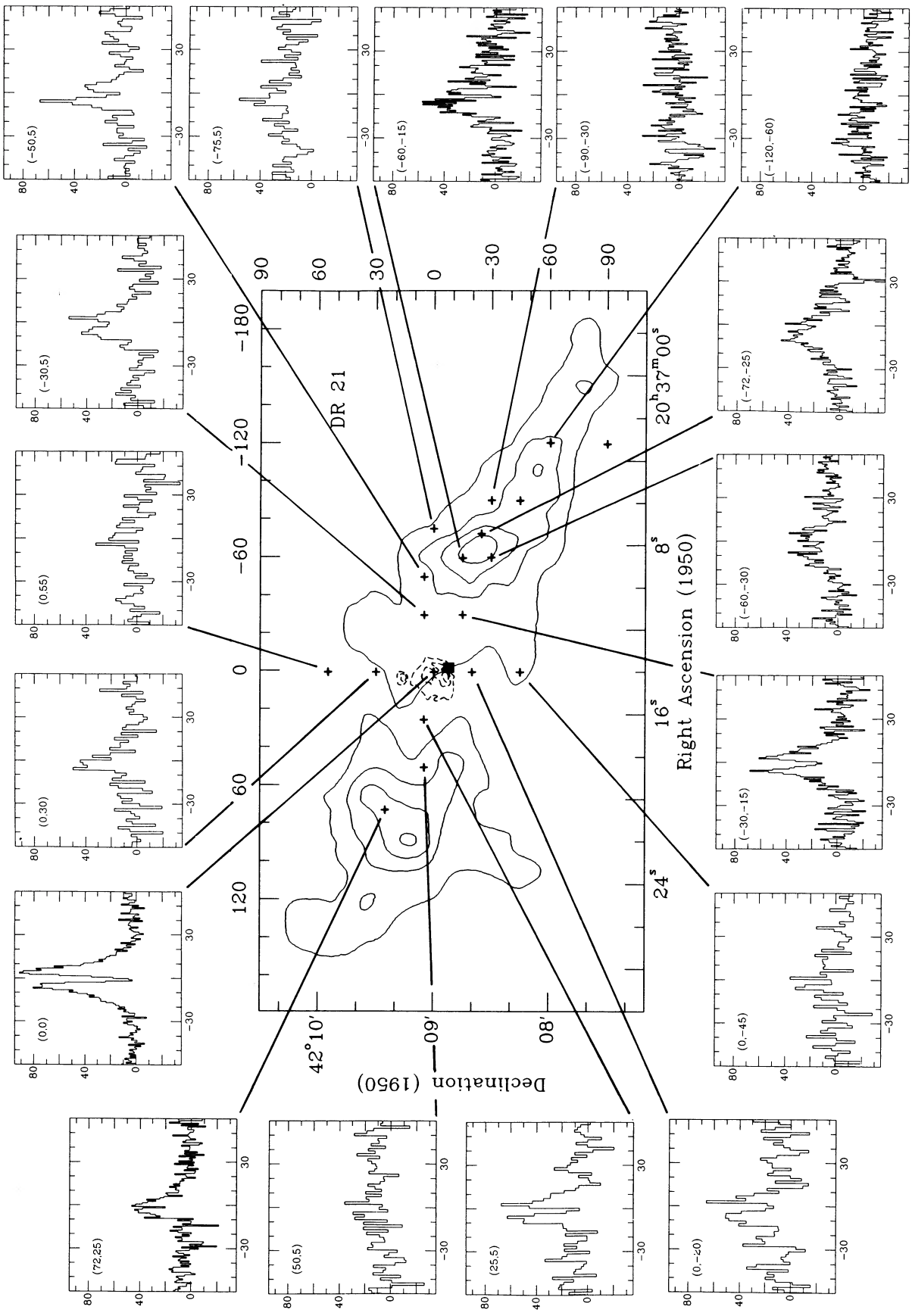

FIG. 2.—CO 7 → 6 spectra toward DR 21. The axes and labels on the spectra are the same as in Fig. 1. The (0, 0) position for the map was $20^h37^m14^s0 + 42°09'00''$ (1950). The center panel is a map of DR 21 showing the distribution of H_2, $v = 1 \rightarrow 0\ S(1)$ line flux (Garden *et al.* 1986, *solid lines*) and the 6 cm continuum emission (Dickel *et al.* 1983, *dotted lines*). The square marks the position of an H_2O maser emission center (Genzel and Downes 1977). Spectra from two positions with nondetections have been omitted to save space.

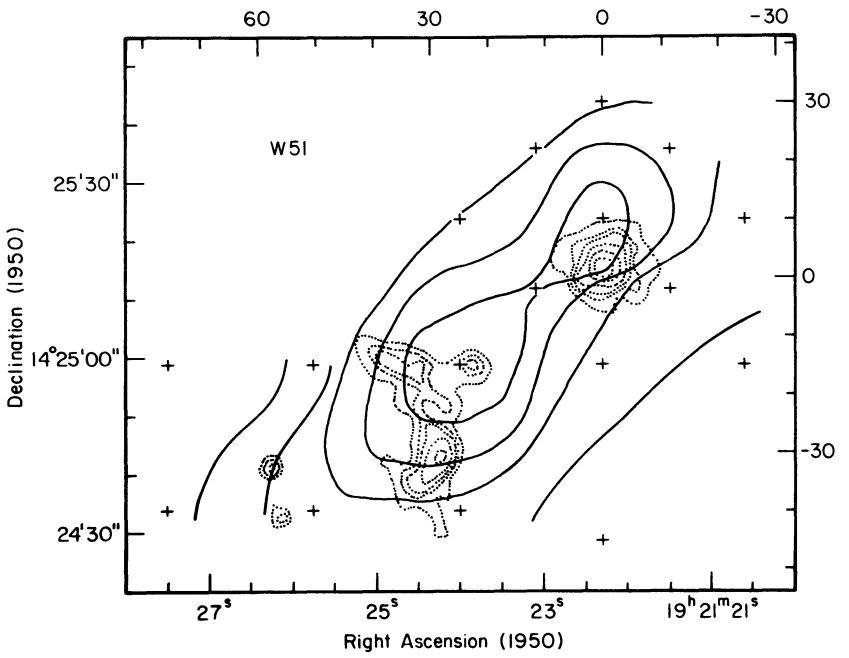

FIG. 3*a*

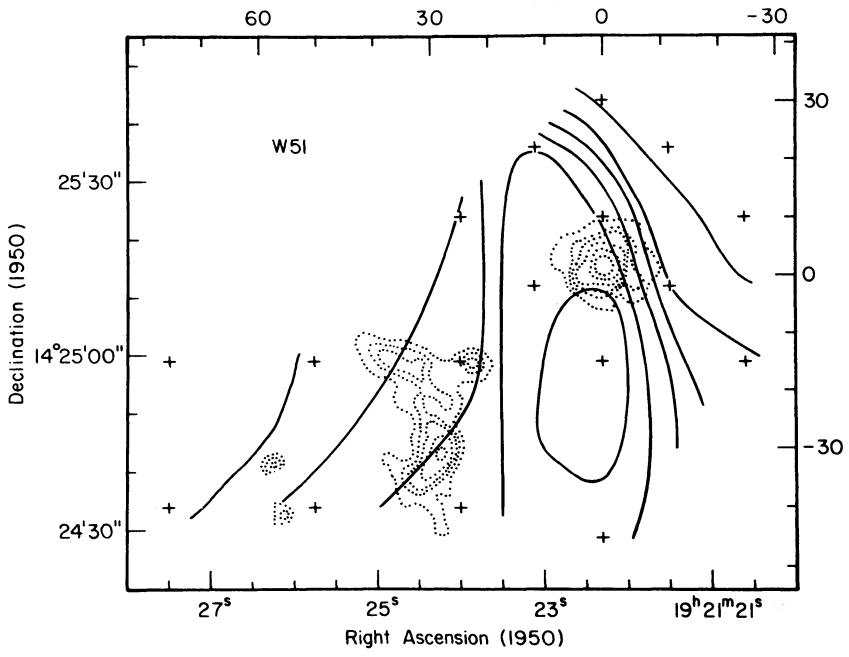

FIG. 3*b*

FIG. 3.—(*a*) Distribution of CO $7 \rightarrow 6$ T_{MB} in W51 (*solid contours*). Contours represent 50, 60, 70, 80, and 90% of the peak temperature of 70 K. The crosses mark the observed positions. The dotted contours show the 1.3 cm radio continuum. (*b*) Distribution of CO $7 \rightarrow 6$ line flux from the broad line component [$\int T\,dv$ – 5 km s^{-1} × T_{MB}] in W51. Contours are 50, 60, 70, 80, and 90% of the peak value (800 K km s^{-1}).

peak value over the whole area mapped in the $7 \rightarrow 6$ line. CO $1 \rightarrow 0$ emission extends over more than 20′ (Mufson and Liszt 1979).

c) W51 Spectra

The CO $7 \rightarrow 6$ spectra toward W51 IRS 2 and W51 MAIN agree well with our earlier spectra of these two sources (JHG). In the $7 \rightarrow 6$ spectrum toward a point 10″ north of IRS 2 (Figure 5), the line has a $\sim$7 km s^{-1} wide peak but extends over 40–50 km s^{-1} above 5 K main beam brightness temperature. The $7 \rightarrow 6$ line has a Planck brightness temperature about 2 times higher than the $2 \rightarrow 1$ brightness temperature toward the same position measured in a similar beam. Near the edges of the smaller $7 \rightarrow 6$ source, this ratio drops to $\sim$1.3.

d) DR 21 Mapping Results

The CO $7 \rightarrow 6$ emission in DR 21 (Fig. 2) comes from a source centered on the H II region and H_2O maser emission

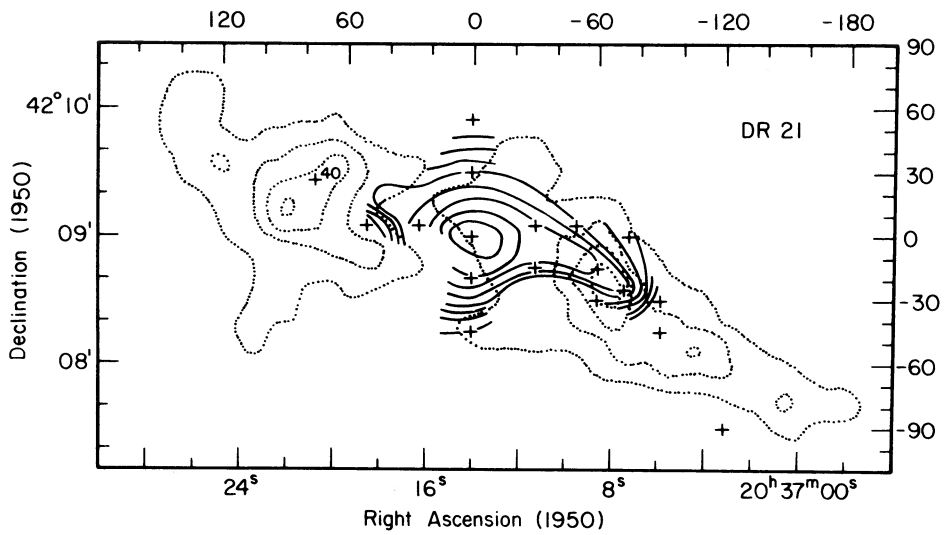

FIG. 4.—Distribution of CO 7 → 6 line flux in DR 21 (*solid lines*). The point labeled "40" has a CO 7 → 6 flux of 40% of the peak value of 1670 K km s^{-1}. The contours are at 10, 20, 30, 40, 50, 60, 70, 80, and 90% of the peak value. The crosses mark the observed positions. The dotted lines show the distribution of the H $v = 1 \rightarrow 0$ $S(1)$ line emission.

center (Harris 1973; Genzel and Downes 1977). The CO 7 → 6 line flux ($\int T\,dv$) distribution (Fig. 4) extends ~130″ (~2 pc, FWHM) northeast and southwest, along the direction of the extended H_2 $S(1)$ emission lobes (Garden *et al.* 1986), but unlike the 2 μm H_2 line, has a peak at the H II region position. The CO 7 → 6 extends only ~60″ (FWHM) in the orthogonal direction. The uncertainty in the line flux due to noise is less than or equal to 5% of the peak flux throughout the region enclosed by contours. Calibration uncertainties may increase the relative errors by up to twice that value. These uncertainties will not affect the large-scale features of the map in Figure 4. There is no readily discernible shift in CO 7 → 6 velocity centroid from northeast to southwest (Fig. 2), although the spectrum at 72″ E, 25″ S shows some excess blue emission when compared to the spectrum at 72″ W, 25″ N. The T_{MB} distribution has a diameter of ~90″ FWHM, significantly less than the size of the 2 → 1 or 3 → 2 CO distributions (this work; Richardson *et al.* 1986). The main-beam brightness temperature is centrally concentrated on the H II region until the 50% contour where there is some extension to the northeast and southwest.

e) DR 21 Spectra

Figure 6 shows three striking results from the CO 7 → 6 spectrum toward the peak of DR 21: (1) the line has a deep ($T_{MB} \leq 5$ K, $T_{PLANCK} \leq 18$ K), narrow ($\Delta v \sim 4$ km s^{-1}) central reversal; (2) the main beam brightness temperature at the highest point in the line is 90 K; (3) the 7 → 6 emission extends over ~50 km s^{-1} above $T_{MB} = 5$ K.

The central reversal in the CO 7 → 6 line extends ~60″ east-west and is compact in the north-south direction (Fig. 2). The reversal is not a result of chopping onto emission. Load-chopped scans of the central position in DR 21 also show this feature. There is also a central reversal in the $J = 2 \rightarrow 1$ line (observed with a 28″ beam vs. 25″ for 7 → 6), but it is both less extended (it appears in the central DR 21 spectrum [Fig. 6] and at positions 25″ west and south) and not as deep ($T_{MB} \sim 22$ K, $T_{PLANCK} \sim 28$ K at the center). The absence of this dip in earlier 2 → 1 and 3 → 2 data (Richardson *et al.* 1985; Plambeck, Snell and Loren 1983) is probably a result of the small absorbing source size and the larger beam sizes in the earlier work. The 2 → 1 dip is also broader ($\Delta v \sim 6$ km s^{-1}) than the 7 → 6 dip. The $CO^{18}O$ $J = 2 \rightarrow 1$ profile has a narrow ($\Delta v \sim 3$ km s^{-1}) emission spike close to the velocity of the CO 7 → 6 dip (Fig. 6). The only other cloud observed so far to have a mild central reversal in the 7 → 6 line is W49 (JHG).

The main beam brightness temperature (90 K; 108 Planck brightness temperature) of the CO 7 → 6 line implies a kinetic temperature in the region of at least 108 K. A conservative estimate of the line peak, allowing for the self-absorption, places a lower limit on the kinetic temperature in the CO 7 → 6 emitting region of 130 K. This is substantially higher than both the temperature implied by the 2 → 1 line (~40 K, this work) or the far-IR dust continuum (~50 K; Harvey *et al.* 1986).

The velocity extent of the 7 → 6 line wings (~50 km s^{-1} at 5% of the peak brightness) is comparable to or greater than the extent of the 2 → 1 line wings (~45 km s^{-1} at 5% of peak brightness). A higher signal-to-noise ratio would most likely reveal an even broader range of emission velocities. The line is symmetric about the central dip and shows no evidence for the redshifted emission from the W75 N cloud which appears at 9 km s^{-1} in the millimeter CO spectra (Dickel, Dickel, and Wilson 1978).

f) Other Sources

The ridge of molecular material running north-south through the DR 21 complex contains two additional luminous sources. In W75 S ($L = 5 \times 10^4\,(D/3\text{ kpc})^2\,L_\odot$; Harvey, Campbell, and Hoffmann 1977), we observed CO 7 → 6 and 2 → 1 toward the near-IR continuum source IRS 1 (Wynn-Williams, Becklin, and Neugebauer 1974), 50″ west of the far-IR source. The 7 → 6 line has a peak T_{MB} of 60 K, about 2.5 times the 2 → 1 brightness temperature (Fig. 8). The strength and shape of the CO 6 → 5 line toward W75 S (Koepf *et al.* 1982) agree with the 7 → 6 line parameters. The line shapes of the 7 → 6 and 2 → 1 lines are in good agreement, with central velocities about 5 km s^{-1} to the blue of the dense core seen in the HCN 4 → 3 transition (White *et al.* 1982). Toward W75 N ($L = 8 \times 10^4\,(D/3\text{ kpc})^2\,L_\odot$; Harvey, Campbell, and Hoffmann 1977), the 7 → 6 line has a brightness temperature of 80 K, ~5

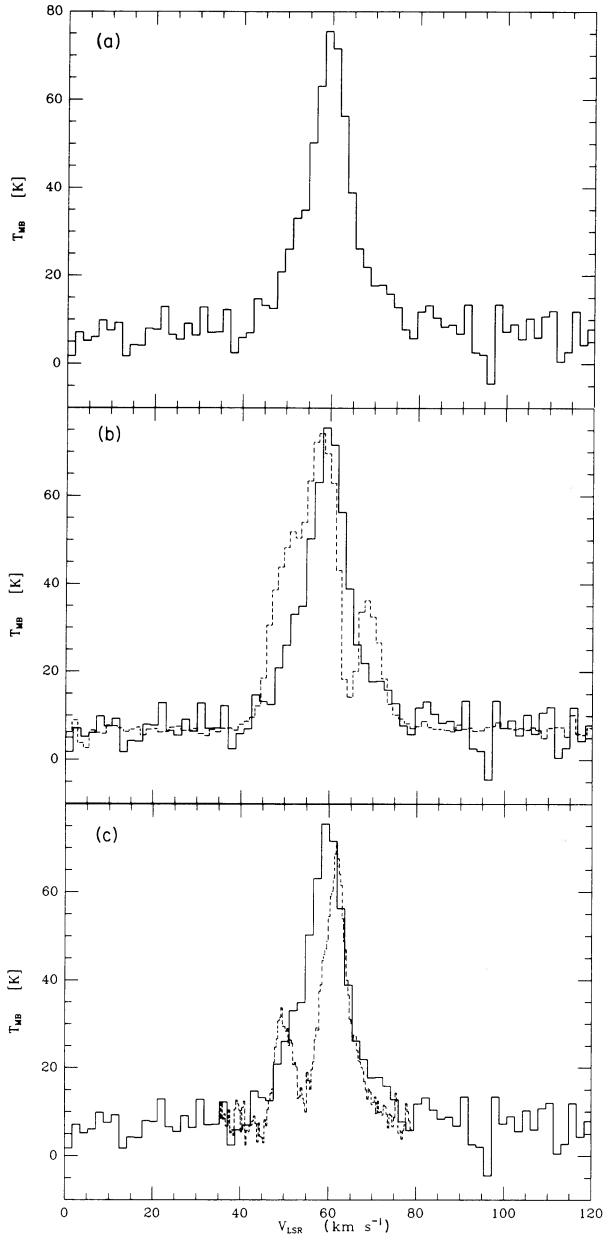

FIG. 5

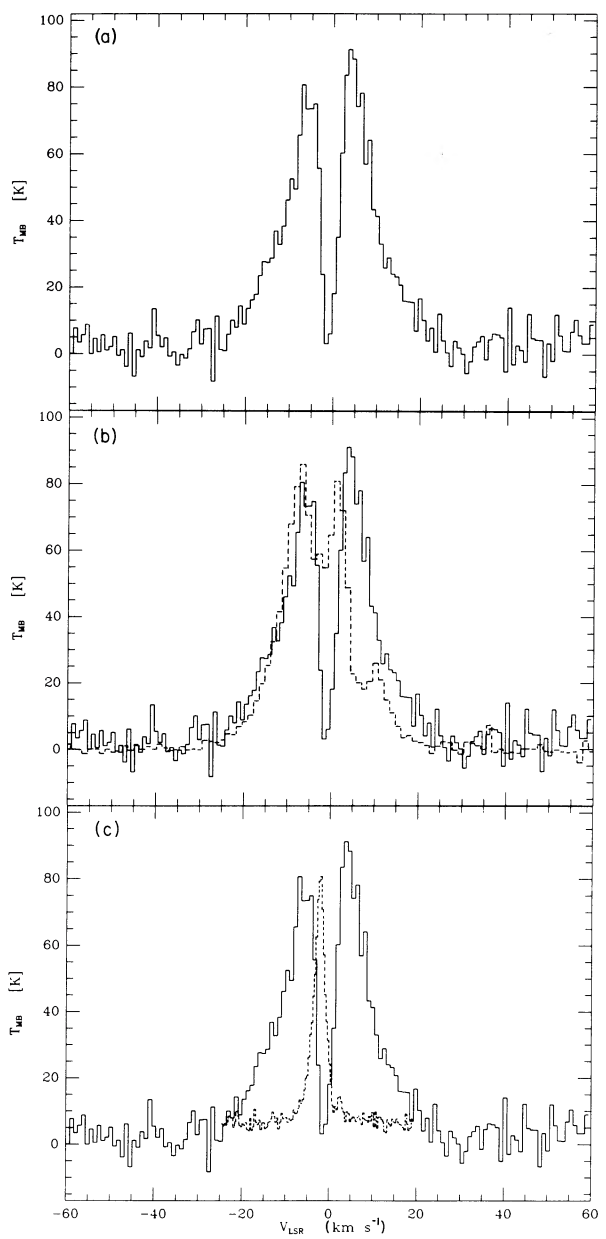

FIG. 6

FIG. 5.—CO spectra toward a point 10″ north of W51 IRS 2. (*a*) CO $7 \rightarrow 6$. (*b*) The dotted line is the CO $2 \rightarrow 1$ spectrum toward the same position taken with a similar beam size (this work, T_R^* multiplied by a factor of 2.1 for comparison). (*c*) The dotted line shows the $^{12}C^{18}O$ $2 \rightarrow 1$ line toward the same position (T_R^* multiplied by 11 for comparison).

FIG. 6.—CO spectra toward DR 21. (*a*) CO $7 \rightarrow 6$. (*b*) The dotted line is the CO $2 \rightarrow 1$ spectrum with T_R^* multiplied by a factor of 3.7 for comparison. (*c*) The dotted line is the $^{12}C^{18}O$ spectrum with T_R^* multiplied by 12 for comparison. The small velocity offset between the CO $7 \rightarrow 6$ absorption dip and the $C^{18}O$ $2 \rightarrow 1$ emission peak is real.

times the $2 \rightarrow 1$ brightness temperature in the same direction (Fig. 7). The center velocity of the $7 \rightarrow 6$ line toward this source is 17 km s^{-1}, about 5 km s^{-1} to the red of the ^{12}CO $2 \rightarrow 1$ line center. The $C^{18}O$ $2 \rightarrow 1$ line from W75 N is at $+10$ km s^{-1}, about the half power point of the $7 \rightarrow 6$ line. The $7 \rightarrow 6$ line profile shows no emission at -2 km s^{-1}, the velocity of the DR 21 cloud at this position (Fischer *et al.* 1985).

IV. DISCUSSION

a) Extended High-Velocity Gas

Both W51 and DR 21 contain CO $7 \rightarrow 6$ high-velocity (total velocity spread >20–50 km s^{-1}) regions which extend over several parsecs. These regions either represent gas which is part of a neutral outflow from the high-luminosity stars forming in the cores of W51 and DR 21, or gas which has been disturbed by a flow of much higher velocity but lower mass. The CO $7 \rightarrow 6$ results are the first indication for an extended high-velocity region in W51. In DR 21, there is a close correspondence between center and orientation of the CO $7 \rightarrow 6$ high-velocity region and those of the large-scale H_2 $v = 1 \rightarrow 0$ source (Fig. 5; Garden *et al.* 1986, 1988).

i) *Distribution of the Broad Line Gas*

In both sources, the high-velocity gas dominates the emergent CO $7 \rightarrow 6$ flux and is centered near the principal lumi-

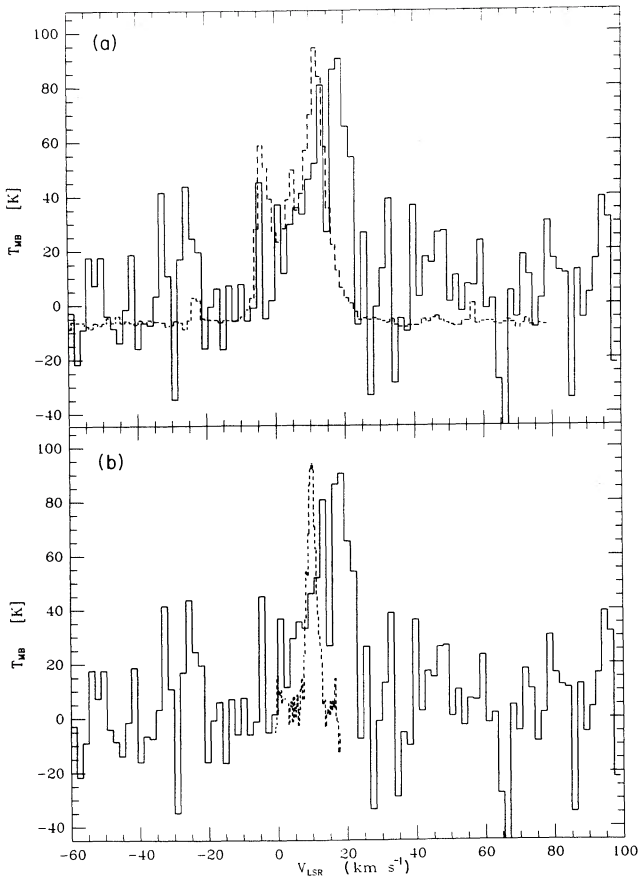

FIG. 7

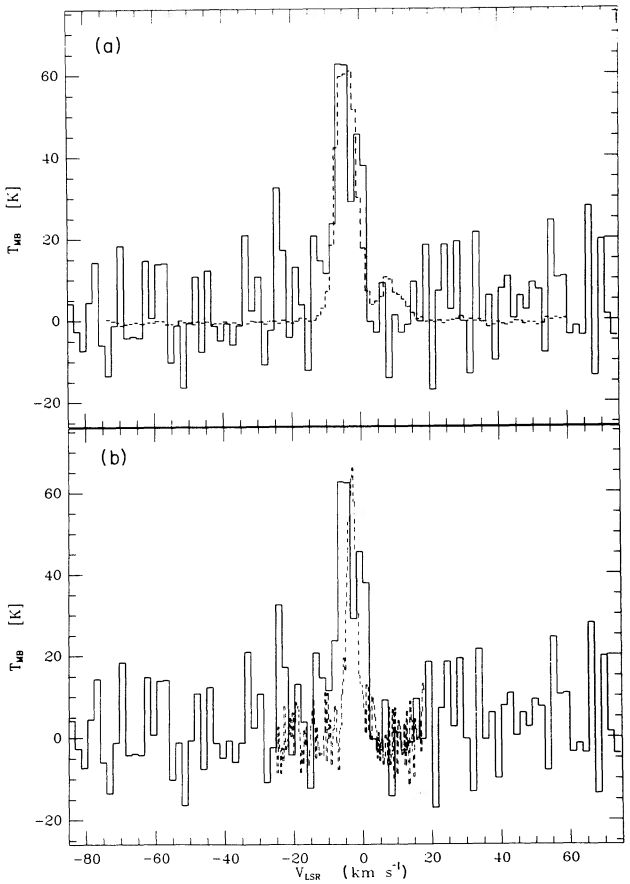

FIG. 8

FIG. 7.—CO spectra toward W75 N. The position for these spectra was $20^h36^m50^s.1$, $+42°26'51''$ (1950). (*a*) CO 7 → 6 (*solid line*) and CO 2 → 1 (*dash-dotted line*, scale is T_R* multiplied by a factor of 5 for comparison). (*b*) CO 7 → 6 and $^{12}C^{18}O$ 2 → 1 (*dash-dotted line*, scale is T_R* multiplied by 18).

FIG. 8.—CO spectra toward W75 S. The position for these spectra was $20^h37^m10^s.1$, $+42°12'00''$ (1950). (*a*) CO 7 → 6 (*solid line*) and CO 2 → 1 (*dash-dotted line*, scale is T_R* multiplied by a factor of 2.5 for comparison). CO 7 → 6 (*b*) and $^{12}C^{18}O$ 2 → 1 (*dash-dotted line*, scale is T_R* multiplied by 25).

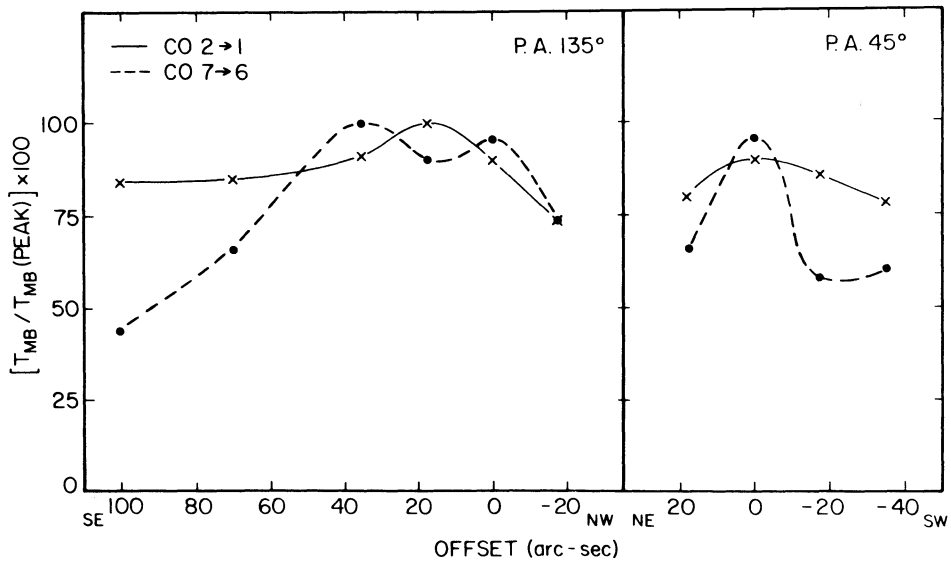

FIG. 9.—Cross-cuts of CO 7 → 6 (*dashed lines*) and CO 2 → 1 (*solid lines*) main beam brightness temperature in W51. The cuts run at position angles of 45° and 135° through (0, 0) = $19^h21^m22^s.3$, $+14°25'25''$ (1950). The maximum likely calibration error (the principal uncertainty from point to point) is ±10% for the 7 → 6 and ±5% for the 2 → 1 observations.

nosity source. In order to estimate how large a contribution the broad-line component makes to the line flux distribution in W51, we fit two Gaussian components to the CO 7 → 6 profiles in the region near IRS 2. Toward the position 10″ north of IRS 2 (Fig. 5), the broad-line component has a FWHM = 18.3 km s^{-1} and accounts for 70% of the total line flux. The narrow component has a FWHM = 6.3 km s^{-1}. Elsewhere in the region, the fits give a width of 20–30 km s^{-1} for the broad component. Overall, the fitting results indicate that about 80% of the CO 7 → 6 line flux from W51 comes from the broad component and about 20% from the bright, narrow-line component. The observed total width and velocity extent of the CO 7 → 6 line probably do not reflect the total velocity range for molecular gas. The width of the CO 16 → 15 line toward IRS 2 (55 km s^{-1}, JHG) is considerably larger than the ~20 km s^{-1} seen in the 7 → 6 line. The presence of CO 2 → 1 emission toward W51 IRS 2 over a velocity range of ~100 km s^{-1} (Stacey *et al.* 1989) shows that the 40–60 km s^{-1} total extent of the CO 7 → 6 line may be an artifact of the signal-to-noise ratio in the weak line wings. Recent high signal-to-noise CO 1 → 0 observations of other molecular flows have shown emission over total velocity ranges up to ~300 km s^{-1} (Lizano *et al.* 1988). Other evidence for broad-line emission from the region around W51 IRS 2 comes from high-velocity H_2O maser emission (Downes *et al.* 1979), from the SiO $v = 0$, $J = 2 \rightarrow 1$ transition which has a similar profile to the CO 7 → 6, with a 7 km s^{-1} wide spike superposed on a ~20 km s^{-1} wide feature (Downes *et al.* 1982), the $NH_3(3, 3)$ line which is ~18 km s^{-1} wide toward IRS 2 (Ho, Genzel, and Das 1983), and the HCO^+ 1 → 0 line which is significantly broader toward IRS 2 than in other parts of the region (Cox *et al.* 1987). Figure 3*b* is a map of the broad-line CO 7 → 6 emission in W51. The strength of the broad component was estimated by subtracting 5 km s^{-1} times the peak line temperature from the line flux at each position to account for the narrow-line emission. The broad component peaks ~15″ south of W51 IRS 2. The emission region is considerably more extended north-south than east-west (≥60″ vs. ~30″ at the 80% level). There is no evidence for a bipolar velocity pattern.

DR 21 also has CO 7 → 6 line emission from both a broad and a narrow component. Most of the emission is from the broad component, as in W51. A two-Gaussian component fit toward the center position in this source (one in emission and one in absorption) fails to explain simultaneously the narrowness of the twin emission peaks and the width at the base of the observed profile (Fig. 6). Other positions near the source center (Fig. 2) may also require a decomposition which includes two emission components. At the position 72″ west, 25″ south of source center, the CO line has a FWHM ~ 25 km s^{-1} and a peak temperature of 40 K. The emission profile from the northeast lobe is similar. This broad line component is most likely reponsible for the large velocity extent of the emission at the central position. The narrow twin peaks are all that remain of emission from the hot quiescent region toward DR 21 after passage through the absorbing gas. Toward the center position, ~75% of the emergent flux is in the broad-line component. The remaining ~25% comes from the unabsorbed part of the quiescent emission component. Elsewhere in the source, the quiescent emission is even less prominent.

Figure 4 is a map of broad-line CO 7 → 6 emission in DR 21. Since there is no evidence for a narrow component at positions away from source center, no correction has been made to the line flux. As in W51, there is no strong evidence for a bipolar velocity pattern. Dust absorption is responsible for the major difference between the broad-line CO 7 → 6 and the 2.12 μm H_2 $v = 1 \rightarrow 0$ $S(1)$ distributions in DR 21. Both are expected to trace the distribution of shock-excited gas. Unlike the H_2, however, the CO 7 → 6 peaks up rather than dropping off in the direction of the H II region and compact far-IR continuum source (Figs. 2 and 4). The same cloud which creates the central hole in the H_2 distribution lies directly toward the molecular ridge (Morris *et al.* 1974) and also causes the CO 7 → 6 narrow-line absorption. Based on our $C^{18}O$ observation, the H_2 column density in the absorbing region is ~6×10^{22} cm^{-2}. This corresponds to a dust optical depth of about 5 at 2.2 μm. The CO 7 → 6 emission extends over greater than 150″ (>2.2 pc at 3 kpc). The broad-line emission is much more prominent in the 7 → 6 line than in the 1 → 0, 2 → 1, and 3 → 2 CO lines (Fig. 6; Richardson *et al.* 1986). In these lower transitions, the cool molecular ridge dominates the emission. The widths and velocities of the CO 7 → 6 and H_2 $S(1)$ line in DR 21 are also remarkably similar over most of the region, although there is some evidence for additional H_2 emission at high velocities (Garden *et al.* 1988).

ii) *Temperature, Luminosity, and Mass of the Broad-Line Gas*

Much of the gas in the broad emission line regions in W51 and DR 21 must have a kinetic temperature in excess of 200 K. Earlier observations of CO 16 → 15 and 7 → 6 toward W51 IRS 2 (JHG) indicated that the high-velocity gas has a temperature of 500–1000 K. Outflowing molecular gas has been observed from this region in the 1.3 cm H_2O maser lines (Schneps *et al.* 1981) and shocked H_2-line emission has also been seen (Beckwith and Zuckerman 1982). We can place a lower limit on the kinetic temperature of the gas at a given velocity and in a given part of the source by comparing the observed brightness temperatures of two or more CO rotational lines to the ratio we would expect for optically thin gas in LTE:

$$\left[\frac{T_{\rm MB}(J_1 \rightarrow J_1 - 1)}{T_{\rm MB}(J_2 \rightarrow J_2 - 1)}\right] = \frac{J_1^2}{J_2^2} \exp\left\{-hB_0 \frac{[J_1(J_1 + 1) - J_2(J_2 + 1)]}{kT_{\rm ex}}\right\}, \quad (1)$$

where J_1 and J_2 are the rotational quantum numbers of the upper level in the higher and lower excitation transition, respectively, B_0 is the rotational constant, and the excitation temperature $T_{\rm ex}$ equals the kinetic temperature. This ratio will be smaller if the line opacity is not small or if the levels are not fully thermalized. For the 7 → 6 and 2 → 1 transitions this ratio is 2 for $T = 75$ K, 4 for $T = 125$ K, 7 for $T = 250$ K, and approaches 12.25 for very high temperatures. Toward W51 IRS 2, the measured value of the main beam brightness temperature ratio at +15 km s^{-1} from the line center is 1.0. At −15 km s^{-1} from line center, the ratio is 5.6. The low ratio on the red side of the line may result from an additional emission component in the cold gas. At 45″ south, the ratios are similar. In DR 21, this ratio at +20 km s^{-1} from line center is 10.5 and at −20 km s^{-1} from line center it is 5. Given the uncertainties in the line calibration (±30%), the lower limit on kinetic temperature is ~100 K for the blueshifted gas in both sources and ~250 K for the redshifted gas in DR 21.

Carbon monoxide in the broad emission line region is an important coolant of the molecular gas in the inner regions of both W51 and DR 21. Integrating over the broad-line com-

ponent and over the source, W51 has a CO 7 → 6 luminosity of 85 $L_\odot$ $(D/7.5\ \mathrm{kpc})^2$ and DR 21 has a luminosity of 31 $L_\odot$ $(D/3\ \mathrm{kpc})^2$. Excitation calculations based on the escape probability formalism show that the corresponding total cooling rate in all CO lines is about an order of magnitude greater than the 7 → 6 cooling rate (the lines arising from states with $J \leq 3$ contribute less than 1% of this total). The relation between CO 7 → 6 and total CO cooling holds for a wide range of excitation conditions. At the highest temperatures possible ($T > 600$ K) for the gas contributing to the 7 → 6 emission, however, the total CO cooling rate could be higher by a factor of 3–6. An overall CO cooling rate of 10^3 $L_\odot$ corresponds to 2–5 × 10^{-4} of the bolometric luminosity derived from the far-IR continuum emission within the corresponding area in W51 (Harvey *et al.* 1986; Jaffe *et al.* 1987). The CO cooling of 300 $L_\odot$ in DR 21 is about 2×10^{-3} of the bolometric luminosity of DR 21 (Harvey, Campbell, and Hoffmann 1977). It is about 20% of the total vibrationally excited H_2 cooling for this region (Garden *et al.* 1986).

The broad CO 7 → 6 emission-line regions in W51 and DR 21 are massive, each containing greater than 170 $M_\odot$ of warm molecular gas. We derive this lower limit from the constraint that, for a given CO column density, there is a well-defined maximum intensity for the CO 7 → 6 line. At low temperatures and densities, the 7 → 6 line has a low brightness temperature, either because it is subthermally excited, or because the gas is cool. At high temperatures and densities, the $J = 7$ level is fully thermalized, but the fixed number of CO molecules will distribute themselves over a large number of possible rotational levels leaving the population in $J = 7$ small. This causes the 7 → 6 transition to be optically thin and the line brightness to be low. We have used our numerical escape probability radiative transfer program for CO to determine quantitatively these minimum column densities. Toward the source center, we require $N_{CO} > 10^{17}$ in W51 and $N_{CO} > 4 \times 10^{17}$ in DR 21 to produce the observed brightness in the broad-line gas. Integrating over the source, this implies a total H_2 mass of greater than or equal to 390 $M_\odot$ for W51 and greater than or equal to 170 $M_\odot$ for DR 21 if $N_{CO}/N_{H_2} = 8 \times 10^{-5}$. If, as is quite likely, the $J = 7$ state is subthermally populated or the 7 → 6 transition optically thick, the H_2 mass could be considerably larger. The masses of these warm high-velocity regions are greater than the masses derived for cooler gas in high-velocity flows in a range of other star-forming regions (Lada 1985). The large amount of warm high-velocity material in W51 and DR 21 implies that this gas could ultimately play a major role in the dispersal of the more diffuse parts of the parent molecular clouds.

iii) *Nature of the Broad-Line Region*

The close morphological and kinematic correspondence of the H_2 $S(1)$ line and CO 7 → 6 emission in DR 21 argues for shock excitation of the molecular gas. The high luminosity of the $v = 1 \rightarrow 0$ $S(1)$ line (180 $L_\odot$; Garden *et al.* 1986) makes fluorescent excitation extremly unlikely. Even the fluorescent models with the largest predicted H_2 line efficiencies can only produce an $S(1)$ luminosity of 10^{-4} of the exciting star, an order of magnitude lower than the observed value in DR 21 (Black and van Dishoeck 1987). MHD shocks, on the other hand, can explain both the H_2 luminosity and the CO luminosity for a wide variety of initial conditions if the shock speed is greater than ~20 km s^{-1} (Draine, Roberge, and Dalgarno 1983; Draine and Roberge 1984).

The main obstacle confronting the shock-excitation model is the elongated appearance of the two sources coupled with the absence of any pronounced bipolarity in the general velocity pattern (see Figs. 1 and 2). This difficulty disappears if both outflows lie in a plane close to the plane of the sky. In this case, a wind from the central luminous object can sweep up material and drive it along at ~20 km s^{-1} to produce the observed broad-line emission. A neutral wind of the order of a few 10^{-4} to 10^{-3} $M_\odot$ per year at 500 km s^{-1} sweeping up neutral material can explain both the luminosity and the minimum momentum flux required by the CO 7 → 6 observations of W51. Even if the bipolar flow is not in the plane of the sky, the interaction of a fast stellar wind with the dense clumps can cause instabilities which lead to significant turbulence in the dense gas. This may be the cause of the observed locally broad lines and may mask any possible bipolar velocity pattern.

b) Warm Quiescent Gas

There is a substantial amount of hot, quiescent gas in W51 and possibly in DR 21. This material has line widths comparable to those seen in millimeter molecular lines, yet has kinetic temperatures well in excess of the far-IR dust temperature. We have analyzed the physical conditions in the hot quiescent gas in M17 and S106 using millimeter, submillimeter, and far-IR CO transitions in an earlier paper (Harris *et al.* 1987*b*). In these regions, the CO 7 → 6 line arises in gas with temperatures of 150–500 K and hydrogen densities between a few 10^4 cm^{-3} and a few 10^5 cm^{-3}. While the strong absorption in DR 21 masks the quiescent gas emission, the maps we present here of CO 7 → 6 toward W51 show clearly the extent of the hot quiescent gas and allow us to compare the distribution of this material to that of other features.

The peak main beam brightness temperature traces the distribution of hot quiescent gas in W51 (Fig. 3*a*). The distribution of T_{MB} supports the conclusion that direct UV heating excites the warm quiescent gas, although excitation by slow shocks cannot be ruled out (Harris *et al.* 1987*b*). Heating by photoelectrons is the most promising direct mechanism, but theoretical calculations fail to account for the observed column densities of warm CO by one to two orders of magnitude (Tielens and Hollenbach 1985; Sternberg 1986). The maps of W51 and DR 21 locate the CO 7 → 6 emission peaks near compact H II regions. The O and B stars in these regions produce the UV photons necessary for production of the high gas temperatures. The extension to the southwest in W51 (Fig. 3*a*) is consistent with this picture because this part of the source not only contains two additional compact H II regions, but also has the highest column densities; i.e., largest number of clumps where photodissociation interfaces can form (Jaffe, Becklin, and Hildebrand 1984).

The extent of the warm CO emission supports the model of warm CO regions as interfaces on a series of clumps in the molecular cloud core (Stutzki *et al.* 1988). The 1 pc by ~3 pc source size in W51 is consistent with the scale lengths for the UV flux passing into the M17 cloud which Stutzki *et al.* (1988) derive from C^+ observations. The source size is considerably larger than can be explained by a single plane-parallel interface.

Arguments similar to those we have used for the broad-line region give a minimum CO column density for the hot quiescent gas toward W51 IRS 2 of a few 10^{17} cm^{-2}. The column density would be about an order of magnitude larger if the source excitation were similar to that in M17 ($T \sim 250$ K, $N_{H_2} \sim 3 \times 10^4$ cm^{-3}; Harris *et al.* 1987). From the 2 → 1 $C^{18}O$

observations, we derive a column density for the cold quiescent CO in the same direction of 2×10^{19} cm^{-2}. The hot gas therefore represents something like 1%–10% of the quiescent material toward IRS 2.

c) *Cold Quiescent Gas*

Some CO $7 \rightarrow 6$ lines from luminous star-formation regions do not have self-reversals even when the millimeter CO lines are strongly self-absorbed (e.g., W49, G34.3 + 0.1; JHG). These results require a pressure discontinuity between the $7 \rightarrow 6$ emitting gas and the absorbing layer to permit the submillimeter emission to pass only through cooler regions where the population in $J = 6$ is extremely low. For CO column densities of $\sim 10^{18}$ cm^{-2} over 3 km s^{-1}, the molecular hydrogen density must be less than 3×10^3 cm^{-3} for $T_k < 50$ K and less than 10^4 cm^{-3} for $T_k < 25$ K (JHG). At these upper limits, the $J = 6$ state is "critically depopulated." Small increases in temperature, pressure, or column density (with the associated excitation increase due to trapping) would result in significant opacity in the cool gas in the $7 \rightarrow 6$ transition.

In DR 21, there are sufficient data available to determine accurately the physical conditions in the self-absorption region if we assume that the temperature and density are uniform. The observations provide us with most of the important information. (1) The self-reversed region is spatially extended in both the $7 \rightarrow 6$ line and the $2 \rightarrow 1$ ^{12}CO line. (2) The dip in the $7 \rightarrow 6$ line, to within the noise, goes to the baseline. The opacity of the absorbing layer is therefore greater than 2 in this line, and the excitation temperature is very low. Also, in spite of the apparent clumpy structure of the cloud (Matsakis *et al.* 1981; Dickel *et al.* 1983), the absorbing layer must have a high area filling factor within our beam (>90%) to account for the total absorption at the center of the $7 \rightarrow 6$ line. (3) Because the absorption takes out both the narrow- and broad-line emission, the absorbing region must lie in front of both emission regions. (4) The region responsible for the CO $7 \rightarrow 6$ absorption is the source of the narrow C^{18}O $2 \rightarrow 1$ emission line (Fig. 6). The CO column density (for $T = 25$ K) is 5×10^{18} cm^{-2}, assuming ^{16}O/^{18}O = 500. (5) The derived CO column density for the absorbing region implies an opacity of about 209 in the $2 \rightarrow 1$ ^{12}CO line. This high opacity accounts for the flat bottom on the reversal of the $2 \rightarrow 1$ profile (Fig. 6) and means that the kinetic temperature of this region must equal the Planck brightness temperature at the center of the $2 \rightarrow 1$ line (28 ± 6 K).

We derive an upper limit to the density in the CO $7 \rightarrow 6$ absorption region ($n_{H_2} < 2 \times 10^4$ cm^{-3}) from the kinetic temperature given by the CO $2 \rightarrow 1$ observations (28 K) and the upper limit to the CO $7 \rightarrow 6$ brightness at the center of the dip (<5 K). Any higher density at this temperature will cause CO $7 \rightarrow 6$ emission from the cool gas which will exceed the observed limit. A geometric argument places a lower limit of 5×10^3 cm^{-3} on the density. If the molecular cloud is not a knife-edge with the edge pointed toward our line of sight to DR 21, the absorbing cloud must have a depth less than 3.5 pc along that line of sight. This distance and the observed column density result in the volume-density lower limit. This density limit further constrains the kinetic temperature since the CO $7 \rightarrow 6$ emission from the absorbing cloud becomes too bright for densities higher than 5×10^3 if the kinetic temperature of the absorption region is greater than 30 K.

Unlike the case of M17 (Stutzki *et al.* 1988), line radiation from the warm quiescent gas does not strongly influence the level populations in the cool foreground layer. The M17 results required a density in the foreground region approaching 10^4 cm^{-3} to cool the CO against radiative pumping from the warm gas. The low-excitation temperatures in the foreground gas in DR 21 may therefore result from the modestly high densities in this region. As in M17, it is unlikely that the foreground cloud could be well enough separated physically from the warm quiescent gas for weak geometric coupling to prevent radiative pumping. The line velocities and widths are too similar. Another reason for the failure of the warm region to radiatively excite the foreground CO could be the large column density of cold material. The resulting high opacity in the cold gas [$\tau(2 \rightarrow 1) \simeq 200$] greatly reduces any possible effects of pumping by CO lines from the warmer background gas.

The sum of all of the information about the absorption region indicates that 22 K < T_{kin} < 30 K, 5×10^3 cm^{-3} < $n_{H_2} < 2 \times 10^4$ cm^{-3}, and the CO column density is 5×10^{18} cm^{-2}. There is a small overlap between the temperature and density of the CO $7 \rightarrow 6$ absorption region in DR 21, and the allowable parameters for the foreground clouds in the other sources we have studied where we saw no CO $7 \rightarrow 6$ absorption. The key difference is the larger column density in the cool gas seen toward DR 21. For a strongly subthermal population in the $J = 6$ level in these clouds, small increases in radiative trapping made possible by additional column density greatly increase the opacity in the $J = 7 \rightarrow 6$ line. (Given the observed CO column density and the derived range of temperatures and densities, the CO $7 \rightarrow 6$ opacity in the cool layer in DR 21 is $2 \leq \tau \leq 30$). The observations are therefore consistent with the regions having very similar temperatures and densities, and only differing in their line-of-sight sizes.

V. CONCLUSIONS

The luminous star-formation regions W51 and DR 21 contain large amounts of molecular gas at temperatures greater than 100–250 K (>250–600 $M_\odot$ under the restrictive assumptions used in our calculations and, most likely, substantially more). Much of this gas is in the form of dynamically active material extending over several parsecs and is either material entrained in or disturbed by protostellar flows. The remaining portion of the warm gas is quiescent. This material has local peaks toward H II regions and the size scale over which it is distributed (1–3 pc) is consistent with a picture of direct ultraviolet heating of molecular cloud boundaries in a highly clumped medium. The DR 21 cloud contains substantial amounts of molecular gas at a density around 10^4 cm^{-3} and a temperature of about 25 K. This cooler material lies along the line of sight to the quiescent region and the core of the high-velocity source.

We are grateful to R. Güsten and J. Howe for help with the observations. D. T. J. acknowledges support from NSF grant AST 8611784 to the University of Texas at Austin.

REFERENCES

Beckwith, S., and Zuckerman, B. 1982, *Ap. J.*, **255**, 536.
Black, J. H., and van Dishoeck, E. F. 1987, *Ap. J.*, **322**, 412.
Cox, M. J., Scott, P. F., Andersson, M., and Russell, A. P. G. 1987, *M.N.R.A.S.*, **226**, 703.
Dickel, J. R., Dickel, H. R., and Wilson, W. J. 1978, *Ap. J.*, **233**, 840.
Dickel, H. R., Lubenow, A. F., Goss, W. M., Forster, J. R., and Rots, A. H. 1983, *Astr. Ap.*, **120**, 74.
Downes, D., Genzel, R., Hjalmarson, A., Nyman, L. A., and Ronnang, B. 1982, *Ap. J.* (*Letters*), **252**, L29.
Downes, D., Genzel, R., Moran, J. M., Johnston, K. J., Matveyenko, L. I., Kogan, L. R., Kostenko, V. I., and Rönnäng, B. 1979, *Astr. Ap.*, **79**, 233.
Draine, B. T., and Roberge, W. G. 1984, *Ap. J.*, **282**, 491.
Draine, B. T., Roberge, W. G., and Dalgarno, A. 1983, *Ap. J.*, **264**, 485.
Fischer, J., Sanders, D. B., Simon, M., and Solomon, P. M. 1985, *Ap. J.*, **293**, 508.
Forster, J. R., Welch, W. J., Wright, M. C. H., and Baudry, A. 1978, *Ap. J.*, **221**, 137.
Garden, R., Geballe, T. R., Gatley, I., Hayashi, M., Hasegawa, T., and Nadeau, D. 1988, preprint.
Garden, R., Geballe, T. R., Gatley, I., and Nadeau, D. 1986, *M.N.R.A.S.*, **220**, 203.
Genzel, R., and Downes, D. 1977, *Astr. Ap. Suppl.*, **30**, 145.
Genzel, R., Becklin, E. E., Wynn-Williams, C. G., Moran, J. M., Reid, M. J., Jaffe, D. T., and Downes, D. 1982, *Ap. J.*, **255**, 527.
Harris, A. I. 1986, Ph.D. thesis, University of California, Berkeley.
———. 1988, *Internat. J. Infrared. Millimeter Waves*, **9**, 231.
Harris, A. I., Jaffe, D. T., Stutzki, J., and Genzel, R. 1987*a*, *Internat. J. Infrared Millimeter Waves*, **8**, 857.
Harris, A. I., Stutzki, J., Genzel, R., Lugten, J. B., Stacey, G. J., and Jaffe, D. T. 1987*b*, *Ap. J.* (*Letters*), **322**, L49.
Harris, S. 1973, *M.N.R.A.S.*, **162**, 5P.
Harvey, P. M., Campbell, M. F., and Hoffmann, W. F. 1977, *Ap. J.*, **211**, 786.
Harvey, P. M., Joy, M., Lester, D. F., and Wilking, B. A. 1986, *Ap. J.*, **300**, 737.
Hildebrand, R. H., Loewenstein, R. F., Harper, D. A., Orton, G. S., Keene, J., and Whitcomb, S. E. 1985, *Icarus*, **64**, 64.
Ho, P. T. P., Genzel, R., and Das, A. 1983, *Ap. J.*, **266**, 596.
Jaffe, D. T., Becklin, E. E., and Hildebrand, R. H. 1984, *Ap. J.* (*Letters*), **279**, L51.
Jaffe, D. T., Genzel, R., Harper, D. A., Harris, A. I., and Ho, P. T. P. 1987, in *IAU Symposium 115, Star Forming Regions*, ed. M. Peimbert and J. Jugaku (Dordrecht: Reidel), p. 143.
Jaffe, D. T., Genzel, R., Harper, D. A., Harris, A. I., and Ho, P. T. P. 1989, in preparation.
Jaffe, D. T., Harris, A. I., and Genzel, R. 1987, *Ap. J.*, **316**, 231 (JHG).
Koepf, G. A., Buhl, D., Chin, G., Peck, D. D., Fetterman, H. R., Clifton, B. J., and Tannenwald, P. E. 1982, *Ap. J.*, **260**, 584.
Kutner, M., and Ulich, B. L. 1981, *Ap. J.*, **250**, 341.
Lada, C. J. 1985, *Ann. Rev. Astr. Ap.*, **23**, 267.
Lellouch, E., Encrenaz, T., and Combes, M. 1984, *Astr. Ap.*, **140**, 405.
Lizano, S., Heiles, C., Rodriguez, L. F., Koo, B. C., Shu, F. H., Hasegawa, T., Hayashi, S., and Mirabel, I. F. 1988, *Ap. J.*, **328**, 763.
Matsakis, D. N., Hjalmarson, A., Palmer, P., Cheung, A. C., and Townes, C. H. 1981, *Ap. J.* (*Letters*), **250**, L85.
Morris, M., Palmer, P., Turner, B. E., and Zuckerman, B. 1974, *Ap. J.*, **191**, 349.
Mufson, S. L., and Liszt, H. S. 1979, *Ap. J.*, **232**, 451.
Plambeck, R. L., Snell, R. L., and Loren, R. B. 1983, *Ap. J.*, **266**, 321.
Richardson, K. J., White, G. J., Avery, L. W., Lesurf, J. C. G., and Harten, R. H. 1985, *Ap. J.*, **290**, 637.
Richardson, K. J., White, G. J., Phillips, J. P., and Avery, L. W. 1986, *M.N.R.A.S.*, **219**, 167.
Schneps, M. H., Lane, A. P., Downes, D., Moran, J. M., Genzel, R., and Reid, M. J. 1981, *Ap. J.*, **249**, 124.
Stacey, G. J., Genzel, R., Harris, A. I., Jaffe, D. T., Lugten, J. B., and Stutzki, 1988, in preparation.
Sternberg, A. 1986, Ph.D. thesis, Columbia University.
Stutzki, J., Stacey, G. J., Genzel, R., Harris, A. I., Jaffe, D. T., and Lugten, J. B. 1988, *Ap. J.*, **332**, 379.
Tielens, A. G. G. M., and Hollenbach, D. J. 1985, *Ap. J.*, **291**, 722.
White, G. J., Phillips, J. P., Beckman, J. E., and Cronin, N. J. 1982, *M.N.R.A.S.*, **199**, 375.
Wynn-Williams, C. G., Becklin, E. E., and Neugebauer, G. 1974, *Ap. J.*, **187**, 473.

R. GENZEL, A. I. HARRIS, and J. STUTZKI: Max-Planck-Institut für Extraterrestrische Physik, D-8046, Garching bei München, Federal Republic of Germany

D. T. JAFFE: Department of Astronomy, R. L. Moore Hall, University of Texas at Austin, Austin, TX 78712

J. B. LUGTEN: Institute for Astronomy, 2680 Woodlawn Drive, Honolulu, HI 96822

G. J. STACEY: Department of Physics, Birge Hall, University of California, Berkeley, CA 94720